ChemPubSoc Europe

DOI: 10.1002/cbic.201500169

CHEMBIOCHEM Communications

VIP

Positional Scanning Synthesis of a Peptoid Library Yields New Inducers of Apoptosis that Target Karyopherins and Tubulin

Glòria Vendrell-Navarro,[a, b] Federico Rúa,[b] Jordi Bujons,[b] Andreas Brockmeyer,[a] Petra Janning,[a] Slava Ziegler,[a] Angel Messeguer,[b] and Herbert Waldmann*[a, c]

We describe the synthesis of a library of 11 638 *N*-alkylglycine peptoid trimers in a positional scanning format with adjustment of reaction conditions to account for different reactivities of the monomer building blocks. Evaluation of the library by high-content phenotypic screening for modulators of the cytoskeleton and mitosis resulted in the identification of two apoptosis-inducing peptoids, which, despite their structural similarity, target different proteins and cellular mechanisms. Whereas one peptoid binds to karyopherins, which mediate nuclear transport, the other *N*-alkylglycine trimer binds tubulin at the vinca alkaloid binding site.

Introduction

Oligomers of *N*-alkylglycine—that is, peptoids—are synthetically rapidly accessible peptidomimetics that allow large and diverse compound libraries to be generated.[1–2] Often, these libraries are synthesised and screened as mixtures of multiple individual library members and require subsequent deconvolution in order for the true active hit compound(s) from the mixtures to be identified.[3] To facilitate hit identification, positional scanning substrate combinatorial libraries (PS-SCLs; positional scanning libraries) were introduced.[4–5] In the synthesis of positional scanning libraries, separate sublibraries are assembled. In the case of peptoids, in each sublibrary an *N*-alkylglycine unit at one position is defined and kept, whereas for the other *N*-alkylglycines random mixtures of all building blocks are introduced (Scheme 1). Thus, each sublibrary serves to "scan" one defined position, and analysis of all sublibraries will reveal the preferred building blocks in each position. To assure efficient hit identification from PS-SCLs, individual building blocks must be equally reactive under the conditions of library synthesis in order to guarantee equal or at least very similar proportions of the different final library members in the generated mixtures. This precondition limits the strategy to transformations in which equal reactivity is assured by appropriate activation techniques[6–7] (e.g., peptide synthesis) or in which only building blocks of limited structural variation and reactivity—and, therefore, also diversity—are introduced in each synthesis step.[8]

A major advantage of PS-SCLs is their suitability for cell-based and in vivo assays.[9–13] However, identification of cellular targets (if unknown) from the identified hits remains a major challenge. In this regard, peptoids in general are cell-permeable,[14] in contrast to the corresponding analogous peptides,[1–2]

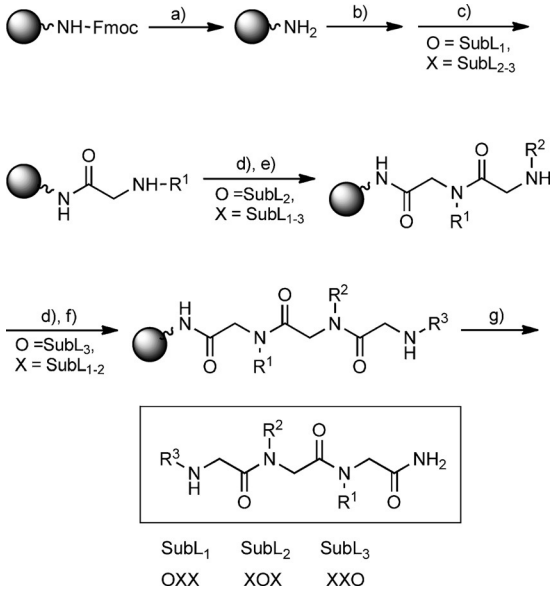

Scheme 1. Solid-phase synthesis of a library of trimers of *N*-alkylglycine derivatives by the submonomer strategy. According to the positional scanning format, the library was divided into three sublibraries (OXX, XOX and XXO, in which O represents a defined position, whereas X refers to a mixture of all amines for this position). Briefly, after removal of the Fmoc protecting group from the Rink amide resin, successive acylation steps with bromoacetic acid followed by the corresponding amination of the bromomethyl intermediate either with the selected individual amine (O) or with the pre-equilibrated mixture of amines (X) were conducted. Finally, treatment of the resin with 60% TFA yielded the final mixtures. a) 20% piperidine, DMF; b) $BrCH_2COOH$/DIC, DMF/CH_2Cl_2; c) R^1-NH_2, DIPEA, DMF; d) $BrCH_2COOH$/DIC; e) R^2-NH_2, DIPEA; f) R^3-NH_2, DIPEA; g) TFA/CH_2Cl_2/H_2O (60:40:2).

[a] *Dr. G. Vendrell-Navarro, A. Brockmeyer, Dr. P. Janning, Dr. S. Ziegler, Prof. Dr. H. Waldmann*
Department of Chemical Biology
Max-Planck-Institut für Molekulare Physiologie
Otto-Hahn-Strasse 11, 44227 Dortmund (Germany)
E-mail: herbert.waldmann@mpi-dortmund.mpg.de

[b] *Dr. G. Vendrell-Navarro, Dr. F. Rúa, Dr. J. Bujons, Prof. Dr. A. Messeguer*
Department of Biological Chemistry and Molecular Modeling
Institut de Química Avançada de Catalunya (IQAC-CSIC)
Jordi Girona 18–26, 08034 Barcelona (Spain)

[c] *Prof. Dr. H. Waldmann*
Lehrbereich Chemische Biologie, Fakultät Chemie
Technische Universität Dortmund
Otto-Hahn-Strasse 6, 44227 Dortmund (Germany)

Supporting information for this article is available on the WWW under http://dx.doi.org/10.1002/cbic.201500169.

and can therefore be used advantageously in cell-based assays. Biological investigation of peptoids has yielded valuable hit compounds covering a wide spectrum of activities,[15–24] thus making them an attractive scaffold for exploration of target identification techniques.

In order to investigate whether the synthesis of peptoid libraries with high structural diversity (relative to previous examples[23–24]) and similar or equal composition of individual library members can be achieved by means of the positional scanning strategy, we report the construction of an improved *N*-alkylglycyl trimer PS-SCL. It is also the first report on the cell-based phenotypic screening of a PS-SCL. We investigated for modulators of cytoskeleton integrity and mitosis, leading to the identification of two apoptosis-inducing peptoids that, despite high structural similarity, exert their biological activity by targeting either tubulin or karyopherins.

Results and Discussion

Reactivity studies and library synthesis

The synthesis of the *N*-alkylglycyl trimer peptoid library followed the submonomer strategy.[25] That is, after attachment of bromoacetic acid to Rink amide resin, repetitive bromoacetamide formation and *N*-alkylation, followed by release from the resin under acid conditions, yielded the peptoid library (Scheme 1). In silico pre-filtering of 3649 commercially available amines according to size, hydrophobicity and potential toxicity was employed to select amines to introduce R^1–R^3 into the library (22 amines for R^1, 23 amines for R^2 and 23 amines for R^3; see the Supporting Information for details). Thus, a maximum of 11 638 individual compounds in 68 controlled mixtures were expected.

In order to assess the relative reactivities of the different amines (Scheme 2), they were subjected to a model substitu-

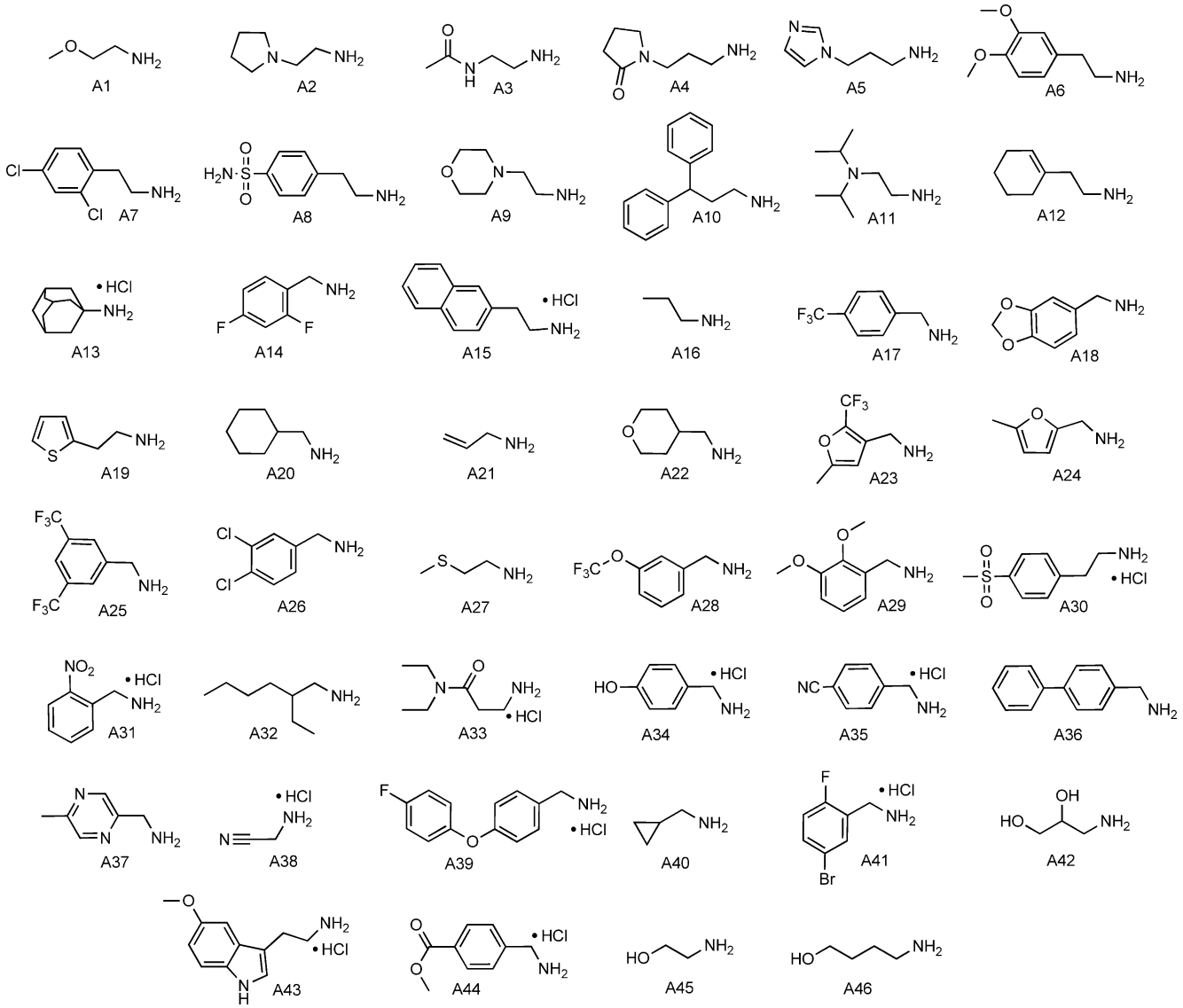

Scheme 2. Collection of 46 primary amines employed for the synthesis of the peptoid library.

tion reaction on resin (Figure S2 in the Supporting Information) and, after release of the alkylation products from the resin, their formation was quantified by HPLC. The corresponding relative reactivity values (RRVs) were applied to assess isokinetic mixtures (see the Supporting Information). Application of amines in excess to the bromoacetamide-functionalised resin led to complete conversion. More highly reactive amines dominated product formation at the expense of those less reactive, and their reactivity differences could not be satisfactorily counterbalanced the corresponding equally reactive assays (data not shown). If, instead, amines were used as the limiting reactants in equimolar amounts, levels of conversion correlated with their expected nucleophilicities, but up to 100-fold differences in reactivity were observed (Table S1). Despite these differences, corresponding assays under equally reactive conditions resulted in at most four unbalanced amines per group, which is a substantial reduction in comparison with the equimolar assays (Table S2).

Notably, if amines incorporating an additional nucleophilic amino group in R^1 and R^2—in particular **A9** and **A11**, for example—are introduced, under the conditions of library synthesis, formation of quaternary ammonium salts on resin can occur.[19] This holds true in particular for the first position, where steric hindrance of the resin might favour intramolecular reactions. To overcome this problem, a different synthesis strategy was followed for the two mixtures containing **A9** or **A11** as defined amines in the first position. In these cases, after introduction of R^1 by nucleophilic substitution, the second *N*-alkylglycine building block was synthesised as a Fmoc-protected monomer that was attached to the first *N*-alkylglycine building block by amide formation (Figure S3).

For library synthesis, several reporter peptoids were included as quality controls. These compounds were obtained routinely with $>90\%$ purity (data not shown). During library construction the reactivities of the individual amines were assessed by means of HPLC analysis by analogy to the method described above. Equimolar incorporation of the amines was less efficient than in previous small-scale assays (Table S1). Because amines were used in limiting quantities, additional amination cycles were required to assure complete conversion (Table S2).

For rapid and convenient monitoring of peptoid formation we explored analysis of the formed peptoid mixtures by ESI-MS, keeping it in mind that mass spectrometric analysis of mixture-based libraries can be riddled with redundancy and consequently with a lack of unequivocal compound characterisation.[26–27] ESI-TOF analysis of the peptoid library allowed identification of 88.1% of the expected products with a precision of 21.5 ppm on average (see Mass Analysis on p. 114 of the Supporting Information). For amines **A9** and **A11** without adaptation of the synthesis strategy as described above, the proportions of successfully identified products were significantly lower. With use of the modified strategy, however, product formation was markedly improved (Figure S4). On the other hand, incorporation of adamantyl residue **A13** hampered further reactions, as evidenced by the abundance of undetected products containing this amine in the first and second position, either defined (Table S4) or in a random mixture (Table S5).

Biological assessment of the peptoid library: Identification of apoptosis inducers

Given the fact that compound mixtures obtained from combinatorial libraries can successfully be employed to identify valuable hits in cell-based assays,[9,13] the 68 mixtures of the peptoid library were subjected to a phenotypic screen (in BSC-1 and HeLa cell lines) that monitors changes in cytoskeleton architecture and DNA (Figure S5).[28] Inspection of the acquired microscope images revealed that some mixtures were cytotoxic at 80 μM in both cell lines and suggested that cell death could be due to apoptosis. Reduction of cell viability was assessed with the WST-1 reagent after treatment of BSC-1 cells for 24 h (Table S6). The apoptotic nature of cell death was confirmed through a caspase 3/7 assay (Figure S6). Eight mixtures were selected on the basis of their potencies in reducing cell viability by inducing apoptosis, and the data obtained for each positional sublibrary identified the active amine residues in each position. On the basis of these results 18 individual compounds were synthesised and evaluated for apoptosis induction in HeLa and BSC-1 cells. All compounds reduced cell viability, with four of them exhibiting IC_{50} values below 10 μM (Table S7). Increases in caspase activity were induced by all compounds, but only compound **P9** caused a significant effect at 2.5 μM (Figures S7 and S8). Thus, **P9** was selected for further biological characterisation (Figure 1).

Structure–activity relationship studies

Derivatives of **P9** were prepared in order to identify the key residues responsible for the activity and to map modifications that might render derivatives inactive. Structure–activity relationship (SAR) information gleaned from the library screening indicated that position R^3 was amenable to modification, because the presence of any one of several residues at this position resulted in a cytotoxic compound (Table 1). Removal of aromatic rings (**P20**, **P28**) or exchange for N-heterocycles (**P24**, **P25**) in R^3 reduced the lipophilicity, but also resulted in decreased activity. By combining modifications made in **P20** and **P25**, inactive derivative **P30** was obtained. Then, to unravel the mechanism of action of **P9**, suitable probes for target identification through affinity-chromatography-based proteomics were synthesised. To this end, attachment of a 4,7,10-trioxatridecanamine unit to the C-terminal end of **P9** yielded **P9A** (Figure 2A), which displayed activity similar to that of **P9** (IC_{50} for inhibition of cell viability 5.5 ± 1.1 μM, Table S8) and induced apoptosis (Figure S9).

Unexpectedly, high-content screening of **P9** derivatives identified compounds with different modes of biological activity. Removal of one phenyl group from R^3 (compound **P28**) or incorporation of an alcohol (compounds **P26**, **P27**) yielded mitosis inhibitors, as detected by the accumulation of round cells with intensely stained DNA and microtubuli (Figure S17). To quantify the mitotic arrest for these derivatives, the mitotic

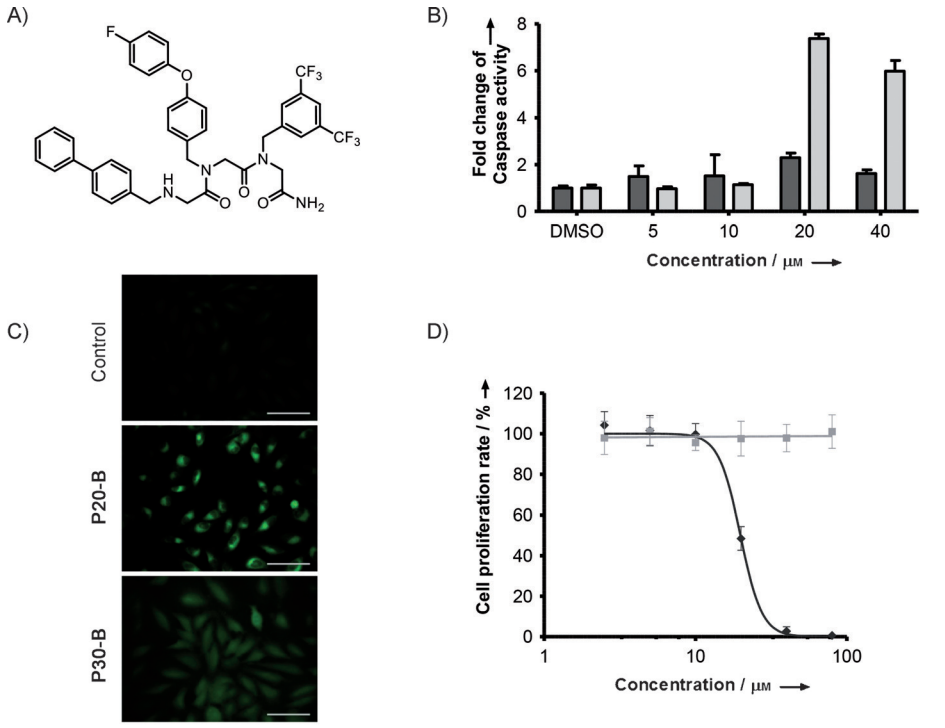

Figure 1. Characterisation of apoptosis induced by **P9**. A) Structure of compound **P9**. B) **P9** increases the activity of caspase 9 but not of caspase 8 in HeLa cells. HeLa cells were treated with different concentrations of **P9** for 3 h. Activities of caspase 8 (■) and caspase 9 (■) were determined through a Caspase-Glo 8 Assay and a Caspase-Glo 9 Assay (Promega), respectively. Data are shown as means ($n=4$) ± s.d.s and are representative of three independent experiments. C) Subcellular localisation of the azido probes in HeLa cells. HeLa cells were incubated for 3 h either with 10 μM of the azido probes or with DMSO as a control. Cells were then fixed and treated with the alkyne reactive mixture to obtain the fluorophore-labelled compounds in cells (green). Untreated cells were also stained with the alkyne reactive mixture as a control. Scale bar: 100 μm. D) Salubrinal protects cells from **P9**-induced cell death. HeLa cells were pre-incubated either with 80 μM Salubrinal (■) or with control medium (◆) for 2 h prior to treatment with different concentrations of **P9** for 4 h. Cell viability was determined with the cell proliferation reagent WST-1. Data are shown as means ($N=4$) ± s.d.s and are representative of three independent experiments.

marker phospho-histone H3 and DNA[29] were monitored. Increases in the mitotic index relative to the DMSO control were detected for derivatives **P26**–**P29** at a concentration of 10 μM, but not for **P9** (Figure S18).

To explore the SAR for mitosis inhibition further, truncated versions of **P9** were prepared (Figure S22). Interestingly, the N-terminal dipeptoid **P32** was inactive whereas the C-terminal dipeptoid **P33** was a mitotic inhibitor with a similar IC_{50} to **P9** (4.4 ± 0.6 μM; Figure S23).

Peptoid **P26** is structurally similar to **P9** and shows similar potency for reduction of cell viability in HeLa cells (Table 1), but through induction of mitotic arrest. Moreover, **P26** was less active in BSC-1 cells (29.0 ± 0.4 μM), whereas **P9** exhibited similar activities in both cell lines (IC_{50} in HeLa cells 4.7 ± 0.3 μM, IC_{50} in BSC-1 cells 4.7 ± 0.4 μM). Induction of apoptosis in the caspase 3/7 activity was observed at 5 μM **P26** (Figure 3D). Because **P26** is structurally related to **P9**, it might have a similar mode of action. Thus, **P9** could be a mitotic inhibitor with increased potency that did not allow formation of round cells at the selected endpoint. Therefore, live-cell imaging of HeLa cells was explored. Typical features of apoptosis (e.g., prolonged period of plasma membrane blebbing, cell shrinkage)[30] were observed early in cells treated with 7.5 μM **P9**, whereas cells treated with 7.5 μM **P26** became rounded after 8–10 h and after 24 h apoptosis was initiated (Movies S1–S3). Under the described conditions, live-cell imaging of **P26**-treated HeLa

Table 1. Derivatisation of **P9** and growth inhibition of HeLa cells. Substituents R^1, R^2 and R^3 in italics are the same as in **P9**. HeLa cells were treated with different concentrations of the compounds for 24 h. Cell viability was determined with the aid of the WST-1 cell proliferation reagent. Data are shown as means ($n=3$) ± s.d.s. Mitotic arrest was assessed by a high-content assay and subsequent automated analysis monitoring the mitotic marker phospho-histone H3 and DNA (Figure S18). See the Supporting Information for additional details.

Product	R^1	R^2	R^3	IC_{50} [μM]	Mitotic arrest
P9	*3,5-bis(trifluoromethyl)benzyl*	*4-(4-fluorophenoxy)benzyl*	*4-phenylbenzyl*	4.7 ± 0.3	no
P19	(3,5-difluorophenyl)methyl	*4-(4-fluorophenoxy)benzyl*	*4-phenylbenzyl*	14.0 ± 0.9	no
P20	*3,5-bis(trifluoromethyl)benzyl*	(4-methoxyphenyl)methyl	*4-phenylbenzyl*	14.4 ± 1.4	no
P21	*3,5-bis(trifluoromethyl)benzyl*	*4-(4-fluorophenoxy)benzyl*	adamantyl	5.2 ± 0.3	no
P22	*3,5-bis(trifluoromethyl)benzyl*	*4-(4-fluorophenoxy)benzyl*	benzyl	18.4 ± 1.0	no
P23	*3,5-bis(trifluoromethyl)benzyl*	*4-(4-fluorophenoxy)benzyl*	methyl	82.8 ± 1.5	no
P24	*3,5-bis(trifluoromethyl)benzyl*	*4-(4-fluorophenoxy)benzyl*	4-pyridinemethyl	27.5 ± 1.9	no
P25	*3,5-bis(trifluoromethyl)benzyl*	*4-(4-fluorophenoxy)benzyl*	4-pyridine	47.3 ± 2.0	no
P26	*3,5-bis(trifluoromethyl)benzyl*	*4-(4-fluorophenoxy)benzyl*	4-hydroxybenzyl	5.7 ± 1.2	yes
P27	*3,5-bis(trifluoromethyl)benzyl*	*4-(4-fluorophenoxy)benzyl*	2-hydroxyethyl	19.5 ± 0.5	yes
P28	*3,5-bis(trifluoromethyl)benzyl*	*4-(4-fluorophenoxy)benzyl*	phenylmethyl	7.9 ± 1.5	yes
P29	*3,5-bis(trifluoromethyl)benzyl*	(4-methoxyphenyl)methyl	phenylmethyl	13.5 ± 1.8	yes
P30	*3,5-bis(trifluoromethyl)benzyl*	(4-methoxyphenyl)methyl	4-pyridine	–	no

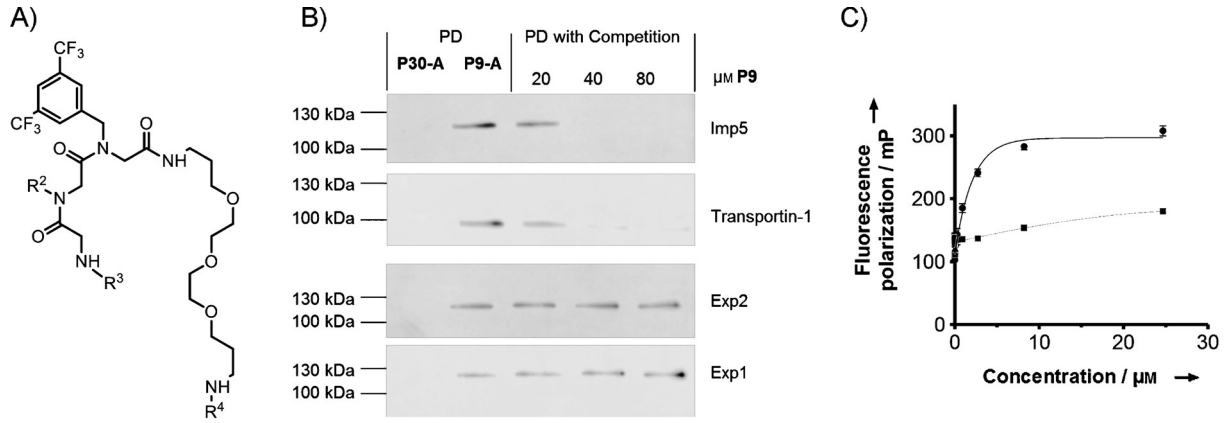

Figure 2. Binding of **P9** to karyopherins. A) General structure of the pulldown probes. Residues R^2 and R^3 differentiate active **P9-A** from inactive **P30-A** and are specified in Figure S9. Amine probes were used for affinity purification ($R^4 = H$), whereas a fluorescein unit ($R^4 = FL$), was incorporated for fluorescence polarisation studies (**P9-D**, **P30-D**). B) Affinity isolation of karyopherins with **P9-A** and **P30-A** probes. Immobilised **P9-A** and **P30-A** were employed for affinity purification with HeLa lysates (PD). Bound proteins were released by specific elution with compound **P9** (pulldown with specific elution). Proteins that remained on the beads were detected by immunoblotting with use of specific antibodies. Results are representative of three independent experiments. C) **P9-D** binds to Imp5. Binding of fluorescent probes **P9-D** (●) and **P30-D** (■) to Imp5 was determined through fluorescence polarisation. The fluorescein-labelled probes were titrated with increasing concentrations of Imp5 until saturation was reached. To calculate K_D values, data were fitted to a one-site binding model.

cells expressing histone 2B-mCherry and α-tubulin-EGFP[31] showed the formation of multipolar spindles and mitotic arrest, whereas **P9**-treated cells showed no mitotic aberrations (Movies S4–S6).

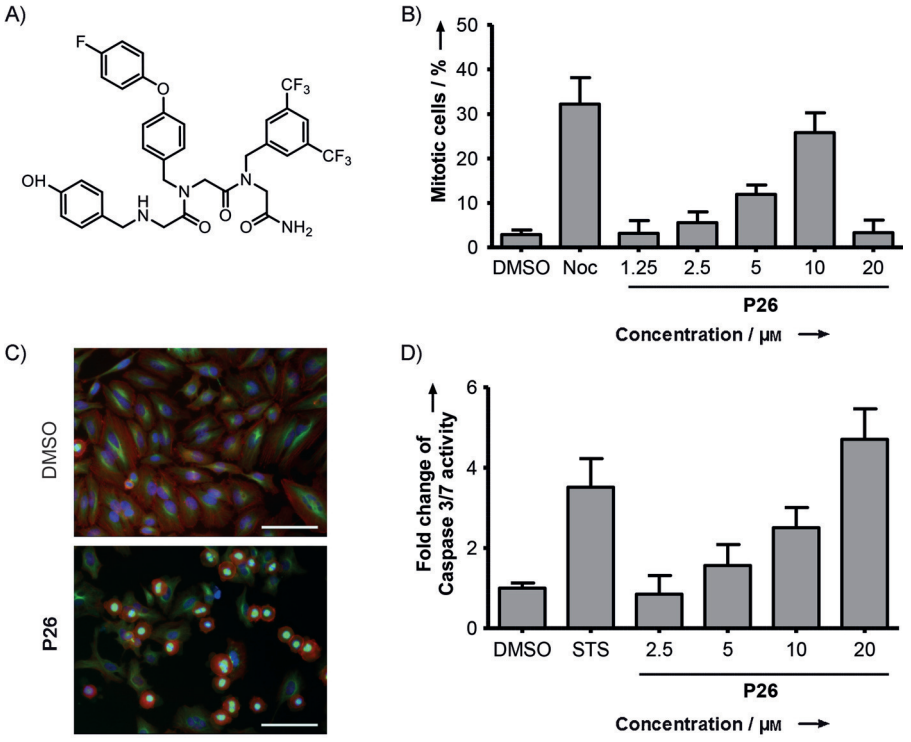

Figure 3. Influence of **P26** on HeLa cells. A) Structure of compound **P26**. B) **P26** increases the number of mitotic cells. HeLa cells were treated for 24 h with the compound or with DMSO and 1 μM nocodazole (Noc) as controls prior to fixation and staining for DNA and the mitotic marker phospho-histone H3 with use of DAPI and anti-phospho-histone-H3 antibody, respectively. High-content analysis was performed to determine the percentages of mitotic cells in the cell populations. Data are shown as means ($n = 3$) ± s.d.s. C) Accumulation of mitotic cells upon treatment with **P26**. HeLa cells were treated for 16 h with 10 μM **P26** or with DMSO as control. Cells were then fixed and stained for microtubules, actin and DNA with α-tubulin antibody coupled to FITC, phalloidin coupled to TRITC and DAPI, respectively. Scale bar: 100 μm. D) **P26** increases caspase 3/7 activity in HeLa cells. Cells were treated for 24 h with different concentrations of **P26** or DMSO or 1 μM staurosporine (STS) as controls. Caspase 3/7 activity was measured through an Apo ONE homogeneous caspase 3/7 assay (Promega). Data are shown as means ($N = 4$) ± s.d.s and are representative of three independent experiments.

The FUCCI sensor is a fluorescent protein-based system that employs cdt1-mKO2 and geminin-mAG1 to visualise the cell cycle.[32] Time-lapse microscopy was employed with FUCCI-transfected HeLa cells to investigate whether **P9**-induced apoptosis is cell-cycle-dependent. However, death occurred to similar extents for G1-phase cells (red) and G2/M cells (green), thus indicating no cell-cycle dependency of the **P9**-induced apoptosis. In contrast, a slight accumulation of cells at the G2/M stage was observed in **P26**-treated cells (Movies S7–S9). Together, these findings indicated that **P9** and **P26** might have different primary cellular targets. Therefore, characterisation of the targeted pathways was explored separately for each compound.

Characterisation of apoptosis induced by P9

The extrinsic death-receptor- and the intrinsic mitochondrial-apoptosis-initiating pathways are characterised by the activation of caspase 8 and caspase 9, respectively. Because treatment of

HeLa cells for 3 h with 20 μM **P9** induced only caspase 9 activity, this compound initiates apoptosis mainly by a mitochondrial pathway (Figure 1B). To gain an insight in the subcellular localisation of potential targets, an in situ fluorescent-dye-generation strategy was applied (Figure S11); this avoids direct influence of the fluorophore on the peptoid localisation. To this end, a benzothiazole-based "click-on" dye was chosen, due to the low affinity of the pro-dye towards proteins or cell organelles,[33] and azido derivatives of **P20** and **P30** (i.e., **P20-B** and **P30-B**, respectively) were prepared. Fixation of **P20-B**-treated cells and a subsequent click reaction resulted in an intense staining of the perinuclear region (Figure 1C), whereas **P30-B**-treated cells displayed a weak fluorescent signal mainly located in the nucleus. **P20-B** was primarily localised in the endoplasmic reticulum (ER) and mitochondria in further colocalisation assays with suitable trackers (Figures S12 and S13).

These results raised the question of whether the **P9**-induced apoptosis was initiated through impairment of the ER functions. Disruption of the ER homeostasis can result in an accumulation of misfolded and unfolded proteins: that is, ER stress. In response to ER stress, cells try to sustain survival through the activation of an integrated intracellular signal transduction pathway termed unfolded protein response (UPR). However, under chronic ER stress cells can undergo apoptosis.[34] Thus, mitochondrial apoptosis can be triggered[35] and consequently accompanied by caspase 9 activation.[36–37] Downstream effectors of the UPR are usually measured as indicators of ER stress.[38] Immunoblotting of a selection of downstream proteins from the IRE1 (inositol-requiring enzyme 1) and PERK (protein kinase RNA-like endoplasmic reticulum kinase) signalling pathways of the UPR[34] was assessed, and only a slight increase in phosphorylated *p*-elf2a was observed (Figures S14 and S15).

Salubrinal is a known stress suppressor that exhibits an anti-apoptotic effect through inhibition of *p*-elf2a dephosphorylation.[39] Interestingly, salubrinal pretreatment protected cells from **P9**-induced apoptosis (Figure 1D).

Identification of cellular targets of P9

To identify the cellular targets of **P9** by means of a proteomics-based approach, probes **P9-A** and **P30-A** were immobilised on NHS-activated Sepharose beads, and both label-free qualitative identification and SILAC-based quantification of proteins enriched during affinity purification ("pulldown") were explored.[40] In the label-free approach, proteins that bound only to the active compound **P9-A** were considered target candidates. SILAC-based identification allows relative quantification of proteins;[41–42] therefore, proteins that were statistically significantly enriched during the affinity purification with the active probe relative to the inactive control were considered hits. Comparison of the results of both strategies revealed several nucleocytoplasmic transport proteins, in particular karyopherins [e.g., importin-5 (Imp5), exportin-1 (Exp1), exportin-2 (Exp2), transportin-1] as potential targets. Because receptor-mediated nucleocytoplasmic transport is essential for cell viability, its disruption can cause cell death.[43] Binding of Imp5, transportin-1, Exp1 and Exp2 to **P9-A** but not to inactive **P30-A** was confirmed by immunoblotting after the pulldown experiment with HeLa lysates. In addition, competition of immobilised and non-immobilised ligand for binding to Imp5 and transportin-1 was observed (Figure 2B). Pulldown experiments employing the purified proteins Imp5, Exp1 and Exp2 instead of cell lysate confirmed binding of the active probe **P9-A** but not of the control probe **P30-A** to all three proteins (Figure S16). In order to monitor binding of **P9** to Imp5 by fluorescence polarisation (FP), fluorescein-labelled derivatives of active **P9** (compound **P9-D**) and inactive **P30** (compound **P30-D**) were employed (Figure 2A) and binding of **P9-D** to Imp5, with an apparent K_D of 1.9 ± 0.1 μM, was confirmed (Figure 2C).

Nuclear export inhibitors such as the Exp1 inhibitor leptomycin B[43] exhibit anticancer activity by disruption of the transport of growth regulatory proteins and of tumour suppressor proteins, and examples of import inhibitors have also been described.[44–45] Proper nucleocytoplasmic protein transport is essential to maintain cell homeostasis. Most of the cargoes identified for each karyopherin use multiple transport pathways to ensure reliable flux through the nuclear pore. Therefore, combined inhibition of several karyopherins might be needed to impair nuclear transport, and this would result in a "fast" apoptotic catastrophe as observed for **P9**.

Target identification for antimitotic derivatives

The antimitotic activity of **P26** was confirmed by quantification as described above[29] (Figure 3B). At 20 μM concentration, apoptotic cell death led to a reduction in the number of mitotic cells. Antimitotic compounds frequently exert their bioactivity by induction of mitotic arrest through interaction with tubulin, and immunostaining of tubulin in the presence of 5 μM **P26** indeed revealed impaired microtubule cytoskeletons in HeLa cells (Figure 4A or Figure S19). Subsequent analysis of tubulin polymerisation through turbidity measurements showed that **P26** dose-dependently inhibited microtubule formation (Figure 4A) and almost completely prevented tubulin polymerisation at a concentration as low as 2.5 μM. In addition, related peptoids **P27**, **P29** and **P33** also inhibited tubulin polymerisation in vitro (data not shown). Peptoid **P9** was again not active in these assays, thus suggesting a different target for this compound. Tubulin polymerisation in cells in the presence of **P26** was monitored through depolymerisation of microtubules by cold treatment and subsequent rewarming at 37 °C to initiate microtubule assembly. In DMSO-treated cells microtubule-organising centres become visible 2 min after rewarming, then microtubules started to regrow 5 min after rewarming, and the microtubule network was recovered after 10 min. In contrast, **P26** delayed the formation of microtubule-organising centres, which appeared 5 min after rewarming.

Of the known binding sites for microtubule-destabilising agents, the colchicine site and the vinblastine site are characterised best.[46] We explored whether **P26** binds to any of these sites through fluorescence-based assays that monitor the displacement of colchicine[47] or BODIPY-FL-vinblastine,[48] respec-

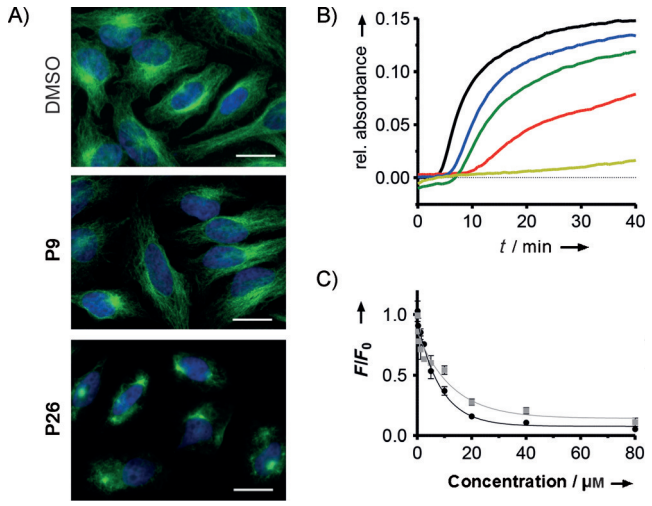

Figure 4. Influence of P26 on microtubules. A) Disruption of the microtubule cytoskeleton is induced by **P26** but not by **P9**. HeLa cells were treated with for 8 h with 5 μM **P9**, 5 μM **P26** or DMSO as control. Cells were then fixed with formaldehyde and stained with DAPI for DNA detection and anti-α-tubulin antibody and Alexa Fluor 488-coupled secondary antibody for microtubule visualisation (see Figure S19 for more details). Scale bar: 20 μm. B) In vitro microtubule formation is inhibited by **P26**. In vitro tubulin polymerisation was evaluated by a turbidity assay. α/β-Tubulin was preincubated at 37 °C with 0.63 (——), 1.25 (——), or 2.50 μM (——) **P26** or DMSO (——) and 1 μM nocodazole (Noc; ——) as controls. Polymerisation was induced with GTP, and absorbance was monitored at 340 nm. The results are representative of three independent experiments. C) **P26** binds tubulin at the vinca alkaloid binding site. A preformed tubulin–BODIPY-FL-vinblastine complex was incubated with either **P26** (■) or vincristine (●) as control at 4 °C. Monomerisation was induced at 37 °C, and fluorescence intensity was monitored at $\lambda_{ex}=490$ nm/$\lambda_{em}=514$ nm. Means ($n=3$) ± s.d.s are depicted relative to the DMSO control.

tively. **P26** does not compete with colchicine for binding to tubulin (Figure S24); however, it displaces BODIPY-FL-vinblastine from tubulin (EC_{50} 9.08 ± 1.50 μM) in a manner similar to the control vincristine (EC_{50} 6.64 ± 1.29 μM; Figure 4). Thus, **P26** is a new tubulin-binding compound that inhibits tubulin polymerisation by binding to the vinca alkaloid site.

Conclusion

We have prepared a PS-SCL of 11 638 *N*-alkylglycine trimers with broad structural diversity and with assured formation of the products in equal or comparable amounts. To this end, building blocks were selected in silico, and their relative reactivities were studied during the construction of the library. Deviations from the expected results highlight the importance of performing in situ controls to identify unequal compositions of the mixtures. Analysis by mass spectrometry turned out to be a useful method to estimate the quality of the library and to identify products that provide valuable information for the deconvolution of the active compounds.

The biological evaluation of the library in a high-content screen monitoring mitosis and the architecture of the cytoskeleton led to the discovery of apoptosis inducers. The selected hit compound **P9** induced fast apoptosis through the mitochondrial pathway. Its effect is inhibited by the ER stress suppressor salubrinal, and it mostly accumulates in the perinuclear area. A proteomics-based approach revealed Imp5, Transportin 1, Exp1 and Exp2 as potential targets of **P9**. Imp5 and Transportin-1, which share import functions, bind a **P9**-derived affinity probe and are specifically eluted with **P9** in excess. A K_D value of 1.9 μM was found for the binding of **P9** to Imp5.

Exchange of the biphenyl ring of **P9** for a phenol unit led to the antimitotic compound **P26**. In vitro, **P26** inhibits tubulin polymerisation and binds to the vinca site of tubulin. However, the strong effect in vitro is not translated into a similarly strong effect in cells, because the compound only partially disrupted microtubule cytoskeleton and only slightly delayed microtubule regrowth in cells.

On the basis of our previous experience,[49–52] the constriction of conformational mobility should improve activity and selectivity of these peptoid hits.

Experimental Section

See the Supporting Information for materials, general synthetic methods, in silico design, procedures, characterisation of compounds and details of the assays.

Acknowledgements

The authors are grateful to Prof. Dr. Dirk Görlich for the Imp5 expression plasmid and helpful discussions, to Christine Nowak for cloning and expression of Imp5 and María José Bleda Hernández for support with the mass analysis. The research leading to our results has received funding from the European Research Council under the European Union's Seventh Framework Programme (FP7/2007–2013)/ERC Grant agreement no. 268309, the Max Planck Gesellschaft and the Spanish Ministry of Science and Innovation (SAF30542-C01–01).

Keywords: apoptosis · combinatorial chemistry · peptidomimetics · peptoids · structure–activity relationships

[1] S. M. Miller, R. J. Simon, S. Ng, R. N. Zuckermann, J. M. Kerr, W. H. Moos, *Bioorg. Med. Chem. Lett.* **1994**, *4*, 2657 – 2662.
[2] P. A. Wender, D. J. Mitchell, K. Pattabiraman, E. T. Pelkey, L. Steinman, J. B. Rothbard, *Proc. Natl. Acad. Sci. USA* **2000**, *97*, 13003 – 13008.
[3] R. A. Houghten, C. Pinilla, J. R. Appel, S. E. Blondelle, C. T. Dooley, J. Eichler, A. Nefzi, J. M. Ostresh, *J. Med. Chem.* **1999**, *42*, 3743 – 3778.
[4] C. Pinilla, J. R. Appel, P. Blanc, R. A. Houghten, *BioTechniques* **1992**, *13*, 901 – 905.
[5] R. A. Houghten, C. Pinilla, M. A. Giulianotti, J. R. Appel, C. T. Dooley, A. Nefzi, J. M. Ostresh, Y. Yu, G. M. Maggiora, J. L. Medina-Franco, D. Brunner, J. Schneider, *J. Comb. Chem.* **2008**, *10*, 3 – 19.
[6] K. L. Dombi, U. E. Steiner, C. Richert, *J. Comb. Chem.* **2003**, *5*, 45 – 60.
[7] T. Ljungdahl, J. Veide-Vilg, F. Wallner, M. J. Tamás, M. Grøtli, *J. Comb. Chem.* **2010**, *12*, 733 – 742.
[8] M. A. Giulianotti, G. Debevec, R. G. Santos, L. E. Maida, W. Chen, L. Ou, Y. Yu, C. T. Dooley, R. A. Houghten, *ACS Comb. Sci.* **2012**, *14*, 503 – 512.
[9] C. Boggiano, N. Reixach, C. Pinilla, S. E. Blondelle, *Pept. Sci.* **2003**, *71*, 103 – 116.
[10] J. Shukaliak Quandt, E. Borras, E. Prat, H. Gelderblom, R. A. Houghten, A. Kashani, C. Pinilla, C.-S. Stuerzebecher, R. Martin, *Mol. Immunol.* **2004**, *40*, 1075 – 1087.
[11] R. A. Houghten, C. T. Dooley, J. R. Appel, *AAPS J.* **2006**, *8*, E371 – E382.

[12] K. J. Reilley, M. Giulianotti, C. T. Dooley, A. Nefzi, J. P. McLaughlin, R. A. Houghten, *Aaps J.* **2010**, *12*, 318 – 329.
[13] L. Onwuha-Ekpete, L. Tack, A. Knapinska, L. Smith, G. Kaushik, T. LaVoi, M. Giulianotti, R. A. Houghten, G. B. Fields, D. Minond, *J. Med. Chem.* **2014**, *57*, 1599 – 1608.
[14] Y. U. Kwon, T. Kodadek, *J. Am. Chem. Soc.* **2007**, *129*, 1508 – 1509.
[15] R. N. Zuckermann, E. J. Martin, D. C. Spellmeyer, G. B. Stauber, K. R. Shoemaker, J. M. Kerr, G. M. Figliozzi, D. A. Goff, M. A. Siani, *J. Med. Chem.* **1994**, *37*, 2678 – 2685.
[16] C. Garcia-Martinez, M. Humet, R. Planells-Cases, A. Gomis, M. Caprini, F. Viana, E. De La Peña, F. Sanchez-Baeza, T. Carbonell, C. De Felipe, E. Pérez-Payá, C. Belmonte, A. Messeguer, A. Ferrer-Montiel, *Proc. Natl. Acad. Sci. USA* **2002**, *99*, 2374 – 2379.
[17] C. Montoliu, M. Humet, J. J. Canales, J. Burda, R. Planells-Cases, F. Sanchez-Baeza, T. Carbonell, E. Perez-Paya, A. Messeguer, A. Ferrer-Montiel, V. Felipo, *J. Pharmacol. Exp. Ther.* **2002**, *301*, 29 – 36.
[18] P. G. Alluri, M. M. Reddy, K. Bachhawat-Sikder, H. J. Olivos, T. Kodadek, *J. Am. Chem. Soc.* **2003**, *125*, 13995 – 14004.
[19] M. Humet, T. Carbonell, I. Masip, F. Sanchez-Baeza, P. Mora, E. Canton, M. Gobernado, C. Abad, E. Perez-Paya, A. Messeguer, *J. Comb. Chem.* **2003**, *5*, 597 – 605.
[20] M. J. Abad-Merin, N. Cortés, I. Masip, E. Pérez-Payá, J. A. Ferragut, A. Messeguer, A. Ferrer-Montiel, *J. Pharmacol. Exp. Ther.* **2005**, *313*, 112 – 120.
[21] B. Liu, P. G. Alluri, P. Yu, T. Kodadek, *J. Am. Chem. Soc.* **2005**, *127*, 8254 – 8255.
[22] G. Malet, A. G. Martin, M. Orzaez, M. J. Vicent, I. Masip, G. Sanclimens, A. Ferrer-Montiel, I. Mingarro, A. Messeguer, H. O. Fearnhead, E. Perez-Paya, *Cell Death Differ.* **2006**, *13*, 1523 – 1532.
[23] H.-S. Lim, C. T. Archer, T. Kodadek, *J. Am. Chem. Soc.* **2007**, *129*, 7750 – 7751.
[24] D. G. Udugamasooriya, S. P. Dineen, R. A. Brekken, T. Kodadek, *J. Am. Chem. Soc.* **2008**, *130*, 5744 – 5752.
[25] R. N. Zuckermann, J. M. Kerr, S. B. H. Kent, W. H. Moos, *J. Am. Chem. Soc.* **1992**, *114*, 10646 – 10647.
[26] N. Yates, D. Wislocki, A. Roberts, S. Berk, T. Klatt, D. M. Shen, C. Willoughby, K. Rosauer, K. Chapman, P. Griffin, *Anal. Chem.* **2001**, *73*, 2941 – 2951.
[27] C. A. Srebalus Barnes, A. E. Hilderbrand, S. J. Valentine, D. E. Clemmer, *Anal. Chem.* **2002**, *74*, 26 – 36.
[28] A. P. Antonchick, C. Gerding-Reimers, M. Catarinella, M. Schurmann, H. Preut, S. Ziegler, D. Rauh, H. Waldmann, *Nat. Chem.* **2010**, *2*, 735 – 740.
[29] V. Eschenbrenner-Lux, P. Küchler, S. Ziegler, K. Kumar, H. Waldmann, *Angew. Chem. Int. Ed.* **2014**, *53*, 2134 – 2137; *Angew. Chem.* **2014**, *126*, 2166 – 2169.
[30] R. C. Taylor, S. P. Cullen, S. J. Martin, *Nat. Rev. Mol. Cell Biol.* **2008**, *9*, 231 – 241.
[31] B. Neumann, T. Walter, J.-K. Hériché, J. Bulkescher, H. Erfle, C. Conrad, P. Rogers, I. Poser, M. Held, U. Liebel, C. Cetin, F. Sieckmann, G. Pau, R. Kabbe, A. Wünsche, V. Satagopam, M. H. A. Schmitz, C. Chapuis, D. W. Gerlich, R. Schneider, R. Eils, W. Huber, J.-M. Peters, A. A. Hyman, R. Durbin, R. Pepperkok, J. Ellenberg, *Nature* **2010**, *464*, 721 – 727.
[32] A. Sakaue-Sawano, H. Kurokawa, T. Morimura, A. Hanyu, H. Hama, H. Osawa, S. Kashiwagi, K. Fukami, T. Miyata, H. Miyoshi, T. Imamura, M. Ogawa, H. Masai, A. Miyawaki, *Cell* **2008**, *132*, 487 – 498.
[33] J. Qi, M.-S. Han, Y.-C. Chang, C.-H. Tung, *Bioconjugate Chem.* **2011**, *22*, 1758 – 1762.
[34] I. Tabas, D. Ron, *Nat. Cell Biol.* **2011**, *13*, 184 – 190.
[35] T. Verfaillie, A. D. Garg, P. Agostinis, *Cancer Lett.* **2013**, *332*, 249 – 264.
[36] M. Boyce, J. Yuan, *Cell Death Differ.* **2006**, *13*, 363 – 373.
[37] E. Szegezdi, D. C. MacDonald, T. Ní Chonghaile, S. Gupta, A. Samali, *Am. J. Physiol. Cell Physiol.* **2009**, *296*, C941 – C953.
[38] C. M. Oslowski, F. Urano, *Methods Enzymol.* **2011**, *490*, 71 – 92.
[39] M. Boyce, K. F. Bryant, C. Jousse, K. Long, H. P. Harding, D. Scheuner, R. J. Kaufman, D. Ma, D. M. Coen, D. Ron, J. Yuan, *Science* **2005**, *307*, 935 – 939.
[40] G. Vendrell-Navarro, A. Brockmeyer, H. Waldmann, P. Janning, S. Ziegler in *Methods in Molecular Biology, Vol. 1263: Chemical Biology* (Eds.: J. E. Hempel, C. H. Williams, C. C. Hong), Springer, New York, 2015, pp. 263 – 286.
[41] S. E. Ong, B. Blagoev, I. Kratchmarova, D. B. Kristensen, H. Steen, A. Pandey, M. Mann, *Mol. Cell. Proteomics* **2002**, *1*, 376 – 386.
[42] J. Cox, M. Mann, *Nat. Biotechnol.* **2008**, *26*, 1367 – 1372.
[43] N. Kudo, B. Wolff, T. Sekimoto, E. P. Schreiner, Y. Yoneda, M. Yanagida, S. Horinouchi, M. Yoshida, *Exp. Cell Res.* **1998**, *242*, 540 – 547.
[44] Y. M. Chook, K. E. Süel, *Biochim. Biophys. Acta - Mol. Cell Res.* **2011**, *1813*, 1593 – 1606.
[45] J. F. Soderholm, S. L. Bird, P. Kalab, Y. Sampathkumar, K. Hasegawa, M. Uehara-Bingen, K. Weis, R. Heald, *ACS Chem. Biol.* **2011**, *6*, 700 – 708.
[46] C. Dumontet, M. A. Jordan, *Nat. Rev. Drug Discovery* **2010**, *9*, 790 – 803.
[47] B. Bhattacharyya, J. Wolff, *Proc. Natl. Acad. Sci. USA* **1974**, *71*, 2627 – 2631.
[48] S. K. Chatterjee, J. Laffray, P. Patel, R. Ravindra, Y. Qin, M. E. Kuehne, S. L. Bane, *Biochemistry* **2002**, *41*, 14010 – 14018.
[49] M. Vidal-Mosquera, A. Fernández-Carvajal, A. Moure, P. Valente, R. Planells-Cases, J. M. González-Ros, J. Bujons, A. Ferrer-Montiel, A. Messeguer, *J. Med. Chem.* **2011**, *54*, 7441 – 7452.
[50] A. Moure, G. Sanclimens, J. Bujons, I. Masip, A. Alvarez-Larena, E. Pérez-Payá, I. Alfonso, A. Messeguer, *Chem. Eur. J.* **2011**, *17*, 7927 – 7939.
[51] M. Corredor, J. Bujons, M. Orzáez, M. Sancho, E. Pérez-Payá, I. Alfonso, A. Messeguer, *Eur. J. Med. Chem.* **2013**, *63*, 892 – 896.
[52] J. Scheper, M. Guerra-Rebollo, G. Sanclimens, A. Moure, I. Masip, D. Gonzalez-Ruiz, N. Rubio, B. Crosas, O. Meca-Cortes, N. Loukili, V. Plans, A. Morreale, J. Blanco, A. R. Ortiz, A. Messeguer, T. M. Thomson, *PLoS One* **2010**, *5*, e11403.

Manuscript received: March 31, 2015
Accepted article published: May 22, 2015
Final article published: June 17, 2015